Journal of Materials Chemistry A

Accepted Manuscript

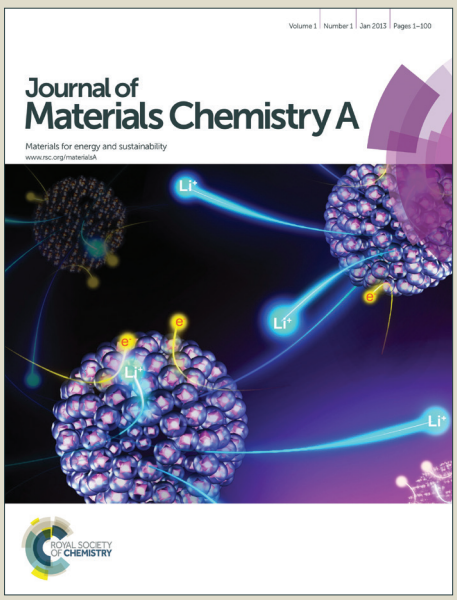

ROYAL SOCIETY OF CHEMISTRY

www.rsc.org/materialsA

Cite this: DOI: 10.1039/c0xx00000x

www.rsc.org/xxxxxx

ARTICLE TYPE

Design of CuO/TiO_2 heterostructure nanofiber and sensing preformance

Jianan Deng, Lili Wang, Zheng Lou and Tong Zhang*

Received (in XXX, XXX) Xth XXXXXXXXX 200X, Accepted Xth XXXXXXXXX 200X
DOI: 10.1039/b000000x

A new type of quasi-1 D nanofiber architecture with heterostructure was prepared via the combination of the electrospinning and hydrothermal strategy in the case of CuO/TiO_2, which showed low operating temperature, high response and excellent selectivity to formaldehyde and ethanol gases.

Nowadays, functional one-dimensional (1D) nanomaterials, including nanorods, nanotubes, nanobelts, and nanowires have attracted intensive attention due to their unique features like low density, the directional mobility of charge carriers, and large aspect ratio.[1-2] All these amazing properties bring them great superiority in a wide variety of applications such as mesoscopic physics and fabrication of nanoscale devices.[3] Particularly, inorganic semiconducting nanostructures have been playing a vital role during the past two decades. Because of their demonstrated or anticipated electrical magnetic, catalytic properties, and unique optical which differ significantly from those of their bulk counterparts.[4-5] These properties of nanostructures not only depend greatly on the materials themselves, such as oxide, chalcogenides, complexes, etc., but also on their characteristics, including sizes, shapes, crystal phases, exposed surface and so on.[6]

As the research moves along, various 1D nanostructures which made of different semiconductor materials have been achieved, and thanks to the deeply and thoroughly study of this kind of single component material system, a variety of stable functioning devices and mature synthesis methods and proven techniques had been verified.[7-8] But sometimes, because of their own physical or chemical characters of the pure nanomaterials, which resulted in their limitations in various properties and affect the performance in application fields. Driven by this, some researchers have begun to study heterogeneous nanostructures, a synthesis of pure materials with novel specialities by manipulating the existing nanoscale object usually are not the only product that achieved during the process, multifunctional heterostructure materials consist of multiple components with various amazing properties in components are also obtained. For example, Gasparotto and Barreca *et al.* have reported that heterostructure has a tremendous potential application. [9-13] Barreca et al.[14] previously reported that decorating porous CuxO matrices onto TiO_2 nanoparticles exhibited very attractive high-rate capabilities and good stability in lithium batteries. They [15] also reported that CuO/TiO_2 nanocomposites functionalized with Au nanoparticles exhibited excellent gas sensing properties. Moreover, In *et al.* [16] recently reported that the hollow nanocubes structured junction between the n-type TiO_2 and p-type CuO could be fabricated by multi-template strategy and exhibited the catalytic performance.

Among various semiconducting materials, TiO_2 and CuO are both technologically important because of their versatile applications.[17] N-type wide band gap semiconductor, due to the outstanding stability in thermal treatment process, photocatalyst procedure and appropriate electronic band structure, Titanium dioxide (TiO_2) have attracted very much attention and welcome in many application fields, such as: humidity/gas sensor, photocatalyst, catalyst supports, energy storage materials and photovoltaic battery.[18] However, TiO_2 possesses large band-gap energy and relatively high resistance thus resulting in limited utilization of applications in the gas sensing field. TiO_2 can be synthesized to improve its sensing performance by introducing of other metal dioxide semiconducting materials, such as ZnO nanosheets and nanorods that we reported before.[19] Cupric oxide (CuO), a p-type semiconductor showed potential applications in diverse fields like magnetic storage, transformational clean-energy technology, electronics, biosensors and chemical sensors, due to its unique optical and magnetic specialities.[20] In 1931, Braver *et al.* discovered that CuO also showed good humidity sensing properties, which made it also the first kind of sensing material that been used in humidity sensing application. Therefore, introducing CuO nanomaterials may be a more economical and reasonable way for enhancing TiO_2 gas sensing performance.[21]

To the best of our knowledge, there have been no reports in the literature on the fabrication of TiO_2 nanofibers (TiO_2 NFs) functionalized with catalytic CuO nanocubes (CuO NCs). Herein, we report a new strategy suitable for the preparation of quasi-1 D p-type CuO nanocubes-loaded TiO_2 heterostructures nanofibers (CuO/TiO_2 HNFs). The fabrication process is a two-step procedure by combining the electrospinning technique and hydrothermal process, and each step is well-controlled (Scheme 1). The gas sensors which made of quasi-1 D heterostructures nanofiber materials were with reduced power consumption and showed enhanced formaldehyde and ethanol-sensing performance.

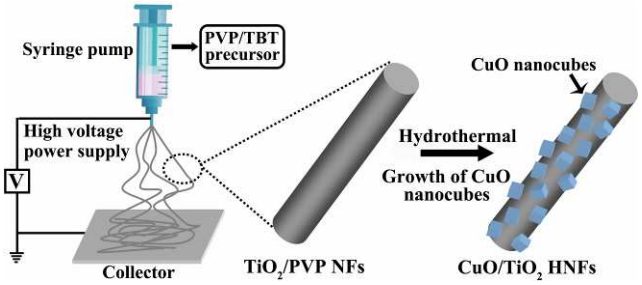

Scheme 1 Schematic illustration of the two processes combined with electrospinning technique for generation of TiO_2 NFs and hydrothermal method for growth of CuO NCs.

In a typical experiment, the TiO_2 NFs were prepared by using the method that our group reported before,[19, 22] which involves electrospinning of a polymer solution mixed with a sol-gel precursor as shown in Scheme 1. And after the heat treatment TiO_2 NFs were obtained. CuO/TiO_2 HNFs were achieved followed by a hydrothermal process that the cupric chloride dehydrate was used as the Cu^{2+} source. The method of preparation the CuO NCs was similar to the preparation of CuO/TiO_2 HNFs, except for the addition of TiO_2 NFs. Specific experimental parameters are shown in Supplementary Information section.

To examine the gas-sensing properties, formaldehyde and ethanol were chosen as the target gas. The structure and circuit diagram of the sensor are shown in Fig. S1(a-b). The main body of a gas senor was a ceramic tube with two Au signal electrodes, each electrode equipped with two Pt wires and coated with above paste. A Ni-Cr heating wire was inserted into the tube to form an indirect-heated gas sensor. Details of the sensor fabrication and test method can be seen in our previous works. [23] And the definitions of the sensing parameters of the sensor are shown in Supporting Information.

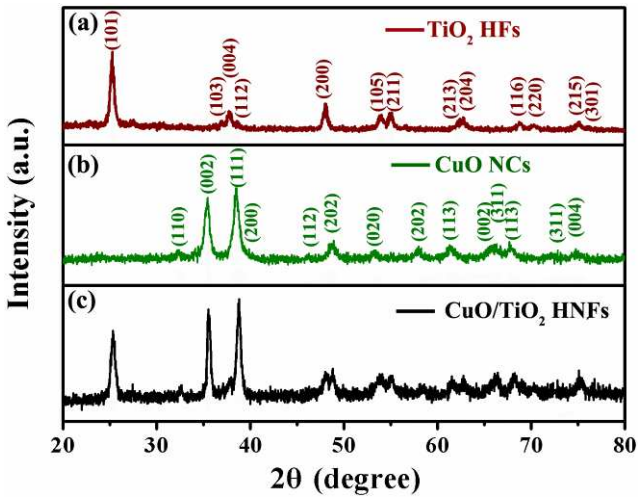

Fig. 1 X-ray diffraction (XRD) pattern of the products: (a) TiO_2 NFs, (b) CuO NCs, and (c) CuO-TiO_2 HNFs.

In order to study the crystal phase of the samples, the X-ray diffraction analysis was also conducted. XRD patterns in Fig. 1 reports the overall phase purity and crystal structure of all the three samples: TiO_2 NFs, CuO NCs and CuO/TiO_2 HNFs. All the diffraction peaks of the pristine TiO_2 (Fig. 1(a)) and CuO (Fig. 1(a)) are both well matched with the JCPDS card of anatase TiO_2 (65-5714) and monoclinic CuO (65-2309). And the diffraction peaks of the CuO/TiO_2 HNFs (Fig. 1(c)) are the combination of individual peaks in the previous two materials. It reveals that the final product consists of the CuO and TiO_2 material.

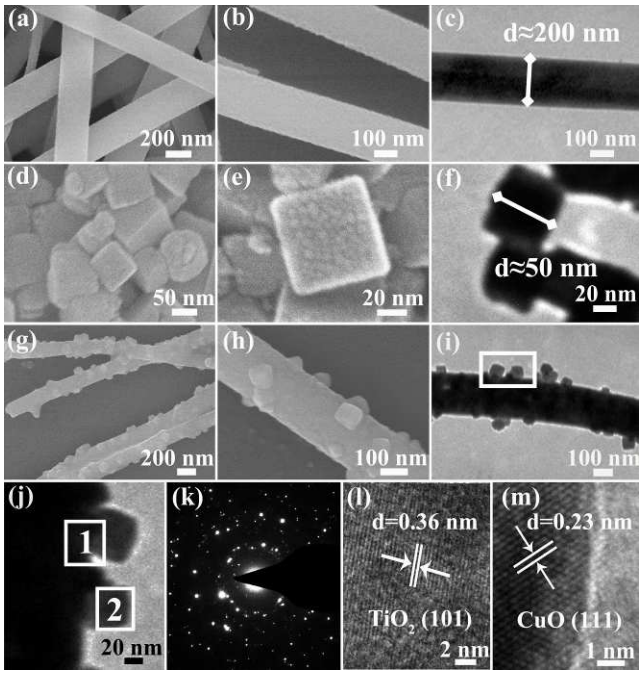

Fig. 2 FESEM and TEM images of the samples: (a-c) TiO_2 NFs; (d-f) CuO NCs; (g-i) CuO/TiO_2 HNFs; (j) higher magnification TEM image of CuO/TiO_2 HNFs; (k) The corresponding SAED pattern; (l and m) HRTEM images taken from spots 1 and 2 in (j), respectively.

The system architecture and nano-organization of samples were observed by FESEM, TEM, SAED and HRTEM. Fig. 2(a-c) showed the obtained pristine TiO_2 non-woven nanofibers were with the diameters about 200 nm, and the surface was relatively smooth without any secondary nanostructures. Fig. 2(d-e) showed the pristine CuO NCs which achieved by the hydrothermal process, the pristine CuO NCs have uniform cube-morphology, with a wide distribution of diameters ranging from 40 nm to 80 nm. The nanocubes appear to be composed by the aggregation of small tiny particles (Fig. 2(e)). A typical TEM image of the CuO samples is shown in Fig. 2(f), where the nanocubes can be clearly seen. After applying the hydrothermal solution growth of the CuO NCs onto the TiO_2 NFs, the hierarchical heterostructures were formed (Fig. 2(g-h)). Sparse densities of secondary CuO NCs that grown on the primary TiO_2 NFs can be clearly seen through the close observation. Careful observations on the surface of the sample (Fig. 2(i)), they show that the quasi-1 D CuO/TiO_2 with loose structures and a few dark spots were observed on the surface of the TiO_2 NF. The high magnification TEM images (Fig. 2(j)) are collected from the individual nanofiber heterostructures (Fig. 2(i), indicated by white squares). It clearly shows the small dark spots are well-regulated and composed of nanocubes with the angles between adjoining sides of 90°. The corresponding SAED pattern (Fig. 2(k)) confirm that the hierarchical CuO/TiO_2 HNFs are polycrystalline structures in nature. Fig. 2(l-m) show HRTEM images of TiO_2 and CuO, respectively, which were recorded from the marked areas in Fig. 2(j) by their corresponding letters. The marked d-spacing value in

Fig. 2(l) is 0.36 nm that corresponds to (101) lattice plane of anatase TiO_2. Similarly, the d-spacing value from Fig. 2(m) is found to be 0.23 nm and it represents (111) planes of monoclinic CuO.

Formaldehyde is one of the most noxious compounds among the volatile organic compounds (VOCs), and predominant symptoms of formaldehyde exposure in humans are irritation of the eyes, nose and throat, together with concentration-dependent discomfort, lachrymation, sneezing, coughing, nausea, dyspnoea and finally death.[24-25] Air pollutants accidents and negative effects on human health may be caused when it leaks out accidentally or by mistake, thus, measurement and control of formaldehyde gas emissions are becoming more and more important.

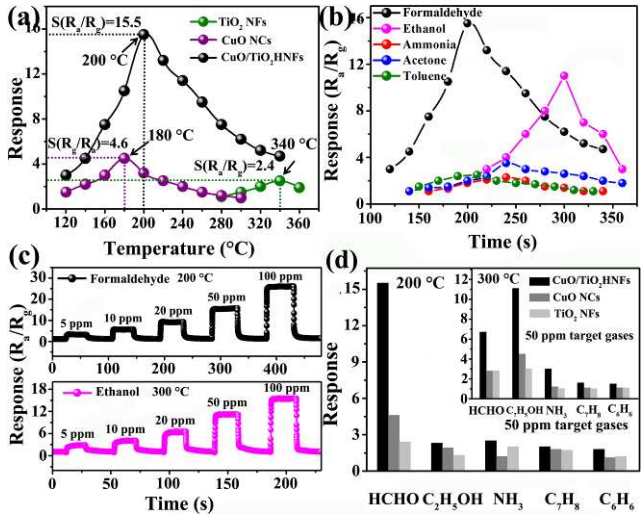

Fig. 3 (a) Responses of pristine TiO_2 NFs, CuO NCs and CuO/TiO_2 HNFs versus operating temperature to 50 ppm of formaldehyde; (b) response of the CuO/TiO_2 HNFs-based sensor to formaldehyde, ethanol, ammonia, acetone, and toluene as a function of operating temperature; (c) response of the CuO/TiO_2 HNFs versus to formaldehyde and ethanol concentrations at 200 and 300 ºC, respectively; (d) response of pristine TiO_2 NFs, CuO NCs and CuO/TiO_2 HNFs versus 50 ppm of various gas vapours at 200 and 300 ºC, respectively.

Working temperature is one of the key factors to a successful gas sensor, the lower the working temperature is, the less power consumption will the sensors take, which also makes the devices last longer and more stable.[26] But some of sensing materials originated from metal dioxide semiconducting materials must sacrifice their working temperature in return for better performance in response and response speed. Fig. 3(a) displays the sensing response curve of three sensors to 50 ppm formaldehyde (HCHO) versus the different working temperature ranging from 120 to 360 °C. The results show that as working temperature increases, the response curve of the three sensors shows "parabola" shape and maximum response values of pristine TiO_2 NFs, CuO NCs and CuO/TiO_2 HNFs are appeared at 340, 180 and 200 °C, respectively. The sensor based on TiO_2 NFs shows no response to formaldehyde under 280 °C, even at its optimum operating temperature of 340 °C, the response of the TiO_2 NFs is only 2.4. The sensor based on CuO NCs got the lowest working temperature at 180 °C with the maximum response of 4.6. Notly, the maximum response of CuO/TiO_2 HNFs made sensor is 15.5, which is about 6.5 and 3.4 times enhancement than the other two.

Furthermore, the relationship between response and operating temperature of the CuO/TiO_2 HNFs-based sensor to 50 ppm of formaldehyde, ethanol, ammonia, acetone, and toluene gases are as shown in Fig. 3(b). It shows that the response of the CuO/TiO_2 HNFs-based sensor to formaldehyde is higher than any other target gases when the operating temperature was set at 200 °C. Moreover, the maximum responses of the sensor at different working temperatures to other target gases are recorded. At 300 °C, the CuO/TiO_2 HNFs-based sensor is found to reach the maximum response of 11.1 to ethanol, which exhibits an enhanced response in comparison with other gases. Interestingly, as the operating temperature was below 275 °C, the sensor based on CuO/TiO_2 HNFs is selective to formaldehyde, while the operating temperature was in the range of 275 to 340 °C, ethanol responses further increase. This feature is potentially advantageous to improve the selectivity of a gas sensor.

The sensing properties of the CuO/TiO_2 HNFs-based sensors to different concentration formaldehyde and ethanol were also investigated (Fig. 3(c) and Fig. S2). It can be seen (Fig. 3(c)) that the response values of the sensors gradually increases as the formaldehyde and ethanol concentration increases. It is worth noting that the CuO/TiO_2 HNFs sensor shows an obvious response even to formaldehyde and ethanol concentration as low as 5 ppm (Fig. S2).

Moreover, the response speed of CuO NCs functionalized TiO_2 NFs sensor is also dramatically increased. The response time values of CuO/TiO_2 HNFs upon exposure to 10 ppm formaldehyde and ethanol are 1.4, and 1.0 s, respectively (Fig. S3), which are the relatively well performance of all related literature (Table 1, in the Supplementary Information section). The CuO/TiO_2 HNFs-based sensor makes a great improvement in response and response/recovery time which attribute to the decoration of CuO NCs. In order to demonstrate the potential use of heterostructures in high response and selective gas sensing, we measured the gas responses (HCHO, C_2H_5OH, NH_3, C_7H_8, and C_6H_6) of the three sensors. Fig. 3(d) depicts the response histogram of the three sensors at 300 (the inset of Fig. 3(d)) and 200 ºC to 50 ppm of target gases. The results indicate that the CuO/TiO_2 HNFs sensor exhibits much more response to HCHO and lesser effects to C_2H_5OH, NH_3, C_7H_8, and C_6H_6 at 200 ºC. Interestingly, when the operating temperature was set to 300 ºC, the CuO/TiO_2 HNFs sensor showed obvious response for C_2H_5OH than that of other gases; implying that the enhancing effect of CuO NCs for gas detection is notable at 200 ºC.

Sensor that based on CuO/TiO_2 HNFs showed excellent sensing performance compare with the pristine ones. The enhancement of the sensing properties can not only owe to the unique quesi-1D heterofibers with hierarchical nanostructures, which can offer plenty of active sites and space for adsorption and reaction between target gases and adsorbed oxygen ions,[27] but also attribute to the p-n junctions that formed in consequence of the synergic electronic interaction between n-type TiO_2 NFs and p-type CuO NCs. In dry air, for pristine TiO_2 NFs, only one layer oxygen adsorbates (O^- or O^{2-}) were formed on the surface of TiO_2.[28] When exposed to target gases, for instance, the formaldehyde molecules will react with the oxygen species on the surface of the TiO_2 NFs, as a result the electrons trapped by the

oxygen adsorbates was then released and rejoined the conduction band. This process explained the increasement of conductivity, and the procedure is depicted in Fig. 4(a) present.[29]

For CuO-modified TiO_2 NFs sensor, by the assistance of CuO, oxygen molecules can be more easily adsorbed on the surface of TiO_2 nanofibers. Because most p-type oxide semiconductors such as NiO, CuO, Cr_2O_3, Co_3O_4, and Mn_3O_4 have been extensively used as good catalysts [30-33] to promote oxygen dissociation. Thus, adsorbed oxygen can diffuse faster to surface vacancies and capture electrons from the conduction band of TiO_2 nanofibers to become oxygen ions. This process not only make a huge increase in the number of adsorbed oxygen but also accelerated the conversion progress between molecule and ion, [34] as a result, the electron depletion of TiO_2 NFs become greater (Fig. 4(b)). Above all, the CuO-modified TiO_2 NFs sensor exhibits remarkably improvement in gas sensing ability in comparison with the single component sensor.

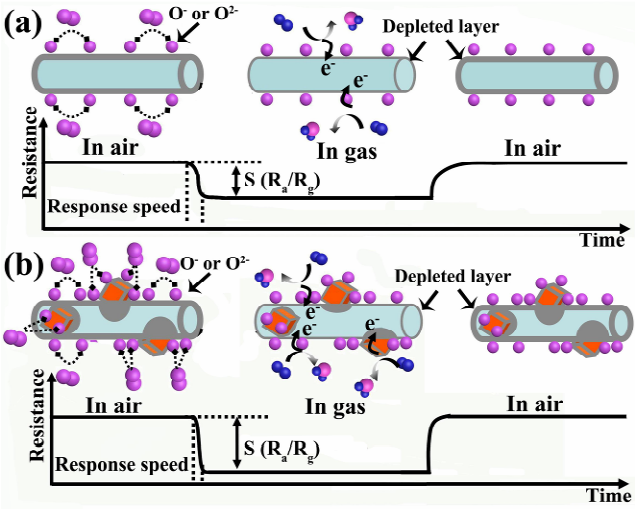

Fig. 4 Schematic diagrams on the gas sensing mechanism of (a) TiO_2 NF and (b) CuO/TiO_2 NF-based sensors.

In summary, a simple two-step method was successfully promoted to synthesize a novel CuO nanocubes-modified TiO_2 HNFs. This method was combination of electrospinning and hydrothermal process. The as-prepared sample consists of CuO NCs with a uniform diameter and TiO_2 NFs with diameter about 200 nm. The CuO/TiO_2 HNFs sensor shows high response, low limit of detection and fast response and recovery towards formaldehyde at the operating temperature of 200 ºC. Importantly, at 300 ºC, the sensor has high response to ethanol. It can be concluded that the CuO/TiO_2 HNFs could exhibit excellent response and selectivity to both formaldehyde and ethanol, only by adjusting the operating temperature, and compared with the individual components, these fantastic heterostructure show a good wealth of outstanding properties that enable them broad applications in catalysis, sensors, Li-ion batteries, micro reactors, biome dicines, and many others.

This research work was financially supported by the Natural Science Foundation Committee (NSFC, Grant No. 51102109), and Project of Innovation Research Team of Jilin University (Grant No. 201004003), the program for Chang Jiang Scholars and Innovative Research Team in University (No. IRT1017), Postdoctoral Science Foundation of China (No. 2012M510878), and Program from Science and Technology Development (No. 20110725).

Notes and references

1 V. V. Sysoev, J. Goschnick, T. Schneider, E. Strelcov and A. Kolmakov, *Nano Lett.*, 2007, **7**, 3182-3188.
2 N. G. Cho, H. S. Woo, J. H. Lee and I. D. Kim, *Chem. Commun.*, 2011, **47**, 11300-11302.
3 Z. Lou, L. Feng, J. N. Deng, L. L. Wang and T. Zhang, *ACS Appl. Mater. Interfaces*, 2013, **5**, 12310-12316.
4 Y. Jiang, W. J. Zhang, J. S. Jie, X. M. Meng, J. A. Zapien and S. T. Lee, *Adv. Mater.*, 2006, **18**, 1527-1532.
5 P. Zhang, C. Shao, Z. Zhang, M. Zhang, J. Mu, Z. Guo and Y. Liu, *Nanoscale*, 2011, **3**, 2943-2949.
6 S. Sen, P. Kanitkar, A. Sharma, K. P. Muthe, A. Rath, S. K. Deshpande, M. Kaur, R. C. Aiyer, S. K. Gupta and J. V. Yakhmi, *Sens. Actuators B*, 2010, **147**, 453-460.
7 J. Q. Hu, Y. Bando and D. Golberg, *J. Mater. Chem.*, 2009, **19**, 330-343.
8 Z. Y. Jin, P. P. Li, G. Y. Liu, B. Z. Zheng, H. Y. Yuan and D. Xiao, *J. Mater. Chem. A*, 2013, **1**, 14736-14743.
9 A. Gasparotto, D. Barreca, C. Maccato and E. Tondello, *Nanoscale*, 2012, **4**, 2813-2825.
10 D. Barreca, A. Gasparotto and E. Tondello, *J. Mater. Chem.*, 2011, **21**, 1648-1654.
11 D. Barreca, G. Carraro, V. Gombac, A. Gasparotto, C. Maccato, P. Fornasiero and E. Tondello, *Adv. Funct. Mater.*, 2011, **21**, 2611-2623.
12 D. Barreca, G. Carraro, A. Gasparotto, C. Maccato, O. I. Lebedev, A. Parfenova, S. Turner, E. Tondello and G. V. Tendeloo, *Langmuir*, 2011, **27**, 6409-6417.
13 D. Barreca, G. Carraro and A. Gasparotto, *Surf. Sci. Spectra*, 2009, **16**, 1-12.
14 D. Barreca, G. Carraro, A. Gasparotto, C. Maccato, M. Cruz-Yusta, J. L. Gómez-Camer, J. Morales, C. Sada and L. Sánchez, *ACS Appl. Mater. Interfaces*, 2012, **4**, 3610-3619.
15 D. Barreca, G. Carraro, E. Comini, A. Gasparotto, C. Maccato, C. Sada, G. Sberveglieri and E. Tondello, *J. Phys. Chem. C*, 2011, **115**, 10510-10517.
16 S. I. In, D. D. V. II and R. E. Schaak, *Angew. Chem. Int. Ed.*, 2012, **51**, 3915-3918.
17 O. Baghriche, S. Rtimi, C. Pulgarin, R. Sanjines and J. Kiwi, *ACS Appl. Mater. Interfaces*, 2012, **19**, 561-564.
18 R. Asahi, T. Morikawa, T. Ohwaki, K. Aoki and Y. Taga, *Science*, 2001, **293**, 269-271.
19 J. N. Deng, B.Yu, Z. Lou, L. L. Wang, R. Wang and T. Zhang, *Sens. Actuators B*, 2013, **184**, 21-26.
20 H. G. Zhang, Q. S. Zhu, Y. Zhang, Y. Wang, L. Zhao and B. Yu, *Adv. Funct. Mater.*, 2007, **17** , 2766-2771.
21 J. T. Zhang, J. F. Liu, Q. Peng, X. Wang and Y. D. Li, *Chem. Mater.*, 2006, **18**, 867-871.
22 Z. Lou, J. N.Deng, L. L. Wang, R. Wang, T. Fei and T. Zhang, *RSC Adv.*, 2013, **3**, 3131-3136.
23 L. L. Wang, H. M. Dou, Z. Lou and T. Zhang, *Nanoscale*, 2013, **5**, 2686-2691.
24 H. Ma, Y. M. Xu, Z. M. Rong, X. L. Cheng, S. Gao, X. F. Zhang, H. Zhao and L. H. Huo, *Sens. Actuators B*, 2012, **174**, 325-331.
25 X. H. Ding, D. W. Zeng, S. P. Zhang and C. S. Xie, *Sens. Actuators B*, 2011, **155**, 86-92.
26 L. L. Wang, T. Fei, Z. Lou and T. Zhang, *ACS Appl. Mater. Interfaces*, 2011, **3**, 4689-4694.
27 J. M. Paik, M. Zielke, M. H. Kim, K. L. Turner, A. M. Wodtke and M. Moskovits, *ACS Nano*, 2010, **4**, 3117-3122.
28 N. Yamazoe, Y. Kurokawa and T. Seiyama, *Sens. Actuators B*, 1983, **4**, 283-286.
29 D. Kohl, *J. Phys. D: Appl. Phys.*, 2001, **34**, R125.
30 H. J. Kim and J. H. Lee, *Sens. Actuators B*, 2014, **192**, 607-627.
31 K. Pirkanniemi and M. Sillanpää, *Chemosphere*, 2002, **48**, 1047-1060.
32 S. S. Kaye and J. R. Long, *J. Am. Chem. Soc.*, 2005, **127**, 6506-6507.
33 Y. Motooka and A. Ozaki, *J. Catal.*, 1966, **5**, 116-124.

34 X. Y. Xue, Z. H. Chen, C. H. Ma, L. L. Xing, Y. J. Chen, Y. G. Wang and T. H. Wang, *J. Phys. Chem. C*, 2010, **114**, 3968-3972.

State Key Laboratory on Integrated Optoelectronics, College of Electronic Science and Engineering, Jilin University, Changchun, 130012, China. Fax: +86 431 85168270; Tel: +86 431 85168385; E-mail: zhangtong@jlu.edu.cn